FOURIER PHASING WITH PHASE-UNCERTAIN MASK

ALBERT FANNJIANG AND WENJING LIAO

Abstract. Uniqueness, up to a global phase, is proved for phasing with a random phase-uncertain mask (PUM). Phasing algorithms alternating between the object update and the mask update are systematically tested and demonstrated to have the capability of recovering both the object and the mask (within the object support) simultaneously with high uncertainty in the mask phases. Phasing with PUM is demonstrated to be robust with respect to the correlation in the mask.

1. Introduction

Fourier phasing is the problem of reconstructing an unknown image from its Fourier intensity data and is fundamental in many applications. Recent breakthroughs center around diffractive imaging of non-periodic objects, combining the penetration power of hard X-ray and the high sensitivity of lensless imaging [3, 17, 22]. Since the interaction of X-rays with matter is weak compared to that of electrons, multiple scattering can be neglected and the singly scattered far field is essentially the Fourier transform of the transmission function of the image via proper choice of variables.

Despite tremendous progresses, many questions, fundamental as well as algorithmic, remain to be solved. The standard phasing algorithms, based on alternating projections [8,11], are plagued by stagnation and spurious errors partly due to intrinsic non-uniqueness of the standard phasing problem. The competition among the true and the ambiguous solutions accounts for their slow convergence and possible stagnation [9, 10].

We believe that the two problems, non-uniqueness and non-convergence, can be solved in one stroke. Our approach is based on Fourier measurement with random mask and yields a unique solution, *up to a global phase factor*, as well as superior numerical performances, including rapid convergence, much reduced data and noise stability. In particular, the random mask method is robust to various types of noise, including Gaussian, Poisson and mask noises, with a noise amplification factor about 2 [5, 6].

Similar in spirit is the wavefront curvature approach [20, 21, 24] which derives uniqueness, up to a global phase, by using cylindrical, in addition to planar, incident waves. The cylindrical wave approach, however, requires $d + 1$ Fourier measurements (d = the dimension of the object) as well as the Neumann boundary condition of Fourier phase. In contrast, our previous uniqueness results [5] require just *one* Fourier measurement for complex-valued objects whose phases are limited to any proper interval $[a, b] \subsetneq [0, 2\pi)$ and *two* Fourier measurements for unconstrained complex objects in any dimension. This is an example of randomized measurement leading to optimal information retrieval. Previously, the effect of a random (binary) mask on Fourier phasing has been observed in [25].

Comparison can also be made with ptychography [3, 15, 22, 23] which is a coherent diffractive imaging method that uses multiple diffraction patterns obtained through the scan of a localized illumination on the specimen. The adjacent illuminations have to overlap around

60 - 70 % in every dimension. This corresponds to at least 3 illuminations for every point of the object and roughly more than 3 Fourier measurements in two dimensions. In fact, random phase mask has been recently deployed in the ptychographic approach to X-ray microscopy to enhance its performance with the extra benefit of reduced dynamic range of the recorded diffraction patterns [16].

A critique that can be leveled against our random mask approach is the use of exact knowledge of the mask which is not always available. We present an approach specifically to the problem of high uncertainty in mask phases that goes well beyond the stability to mask errors demonstrated already in [6]. We will show that *nearly perfect* recovery can be achieved with high uncertainty in mask phases.

We extend two uniqueness results of [5] to the present setting with phase-uncertain mask (PUM). Instead of running phasing algorithms with a fixed erroneous mask, we design algorithms to recover the object and the mask simultaneously. At each iteration, the object and the mask are updated alternatively, aiming at fitting the object constraint, the mask constraint as well as the Fourier intensity data. As shown below our numerical schemes can accurately recover the object with close to 50% uncertainty in mask phases.

The paper is organized as follows. We state the uniqueness theorems for phasing with a random PUM in Section 2 and give the proofs in Appendices A and B. We discuss the basic algorithm of Alternating-Error-Reduction (AER) and prove the residual reduction property in Section 3 and Appendix C. We discuss the Douglas-Rachford-Error-Reduction (DRER) algorithm in Section 4 and the algorithms with two sets of Fourier intensity data in Section 5. We present numerical results in Section 7 and conclude in Section 8. A preliminary version of the results is given in [7].

2. Uniqueness

The effect of a mask amounts to changing the original object f to the masked object

$$g(\mathbf{n}) = \mu(\mathbf{n}) f(\mathbf{n}), \quad \mathbf{n} \in \mathbb{Z}^d \tag{1}$$

where μ is an array representing the mask and d is the dimension. In the standard phasing problem the uniform mask (UM) with $\mu \equiv 1$ is used. In our approach the mask μ is random and only roughly known. In this paper, we will focus on the case of phase masks

$$\mu(\mathbf{n}) = \exp(i\phi(\mathbf{n})), \quad \phi(\mathbf{n}) \in [0, 2\pi), \ \mathbf{n} \in \mathbb{Z}^d \tag{2}$$

We assume that the true phase angles $\phi(\mathbf{n})$, in radian, of the *unknown* mask lie within $\delta\pi$ from the *given* initial estimates $\phi_0(\mathbf{n})$ for all $\mathbf{n}$, i.e.

$$\phi(\mathbf{n}) \in [\![\phi_0(\mathbf{n}) - \delta\pi, \phi_0(\mathbf{n}) + \delta\pi]\!]. \tag{3}$$

Here and below we adopt the following notation: $\theta \in [\![a, b]\!]$ means

$$\begin{cases} a(\mathrm{mod}\, 2\pi) \le \theta(\mathrm{mod}\, 2\pi) \le b(\mathrm{mod}\, 2\pi) & \text{if } a(\mathrm{mod}\, 2\pi) \le b(\mathrm{mod}\, 2\pi) \\ a(\mathrm{mod}\, 2\pi) \le \theta(\mathrm{mod}\, 2\pi) < 2\pi \text{ or } 0 \le \theta \le b(\mathrm{mod}\, 2\pi) & \text{else} \end{cases}.$$

For ease of notation, we shall write below the inequality (3) as $\phi(\mathbf{n}) \in [\![\phi_0(\mathbf{n}) \pm \delta\pi]\!]$.

Let $\mathbf{n} = (n_1, \ldots, n_d) \in \mathbb{Z}^d$ and $\mathbf{z} = (z_1, \ldots, z_d) \in \mathbb{C}^d$. Define the multi-index notation $\mathbf{z}^{\mathbf{n}} = z_1^{n_1} z_2^{n_2} \ldots z_d^{n_d}$. Let $\mathcal{C}(\mathcal{N})$ denote the set of finite complex-valued functions on $\mathbb{Z}^d$ vanishing outside $\mathcal{N} = \{\mathbf{0} \le \mathbf{n} \le \mathbf{N}\}, \mathbf{N} = (N_1, N_2, \ldots, N_d)$. Here $\mathbf{m} \le \mathbf{n}$ if $m_j \le n_j, \forall j$. Set

$|\mathcal{N}| = \prod_{j=1}^{d}(N_j+1)$. An object is said rank ≥ 2 if the convex hull of its support has a dimension ≥ 2.

The $\mathbf{z}$-transform $F(\mathbf{z}) = \sum_{\mathbf{n}} f(\mathbf{n})\mathbf{z}^{-\mathbf{n}}$ of $f \in \mathcal{C}(\mathcal{N})$ is an analytic continuation, from the d-dimensional torus, of the the Fourier transform for $\mathbf{z} = (\exp(2\pi i\omega_1), \ldots, \exp(2\pi i\omega_d)), \omega_j \in [0,1]$.

If the absolute value of the Fourier transform is sampled on the lattice

$$\mathcal{L} = \left\{\boldsymbol{\omega} = (\omega_1, ..., \omega_d) \mid \omega_j = 0, \frac{1}{2N_j+1}, \frac{2}{2N_j+1}, ..., \frac{2N_j}{2N_j+1}\right\} \tag{4}$$

then the autocorrelation function $\mathcal{C}_f(\mathbf{n}) = \sum_{\mathbf{m}\in\mathcal{N}} f(\mathbf{m}+\mathbf{n})\overline{f(\mathbf{m})}$ is uniquely determined. Roughly half of the frequencies in each dimension are harmonic and half are non-harmonic. Hence sampling on $\mathcal{L}$ corresponds to the oversampling ratio $\sigma = |\mathcal{L}|/|\mathcal{N}| \approx 2^d$.

However, the uniqueness of the autocorrelation given the Fourier intensity data does not imply the uniqueness of the object.

First, there are three types of *global* ambiguities: (a) constant global phase, $f(\cdot) \longrightarrow \exp(i\theta)f(\cdot)$, for some $\theta \in [0, 2\pi)$, (b) spatial shift, $f(\cdot) \longrightarrow f(\cdot + \mathbf{m})$, for some $\mathbf{m} \in \mathbb{Z}^d$, (c) conjugate inversion, $f(\cdot) \longrightarrow \overline{f(\mathbf{N} - \cdot)}$. Conjugate inversion produces the so-called twin image.

Our basic tool is the following improved result of irreducibility [12, 13] with, however, a more practical and useful perspective.

Proposition 1. [5] *Let f be a finite complex-valued object of rank ≥ 2. Let $\{\mu(\mathbf{n})\}$ be continuous random variables on nonzero real algebraic varieties $\{\mathcal{V}(\mathbf{n})\}$ in $\mathbb{C}(\simeq \mathbb{R}^2)$ with an* absolutely continuous *joint distribution with respect to the standard product measure on $\prod_{\mathbf{n}\in\Sigma}\mathcal{V}(\mathbf{n})$ where $\Sigma \subset \mathbb{N}^d$ is the support set of f. Then the $\mathbf{z}$-transform of the masked object (1) is irreducible up to a power of $\mathbf{z}^{-1}$ with probability* 1.

The main point here is that while the classical result [12, 13] works for generic (thus random) objects from a certain ensemble Proposition 1 deals with a *given, deterministic* object of rank ≥ 2. This improvement is achieved by endowing the probability measure on the ensemble of masks, which we can manipulate, instead of the space of objects, which we can not control, as in the standard setting.

As a consequence of Proposition 1, the global ambiguities are the sole ambiguities possible as far as the masked object (1) is concerned [12].

This is not all. We are able to remove all ambiguities, with the only exception of a global phase, for the original object f even when the random mask is only roughly known.

Theorem 1. *Let f be a real-valued object of rank ≥ 2. Suppose the exact mask phases $\{\phi(\mathbf{n})\}$ are independently and uniformly distributed on $[-\gamma\pi, \gamma\pi)$. Suppose the uncertainty of the mask estimate $\mu_0 = \{\exp(i\phi_0(\mathbf{n}))\}$ in (3) is $\delta < \gamma/2$.*

Suppose that another real-valued image $\tilde{f}$ and mask estimate $\tilde{\mu} = \{\exp(i\tilde{\phi}(\mathbf{n}))\}$ satisfying

$$\tilde{\phi}(\mathbf{n}) \in [\![\phi_0(\mathbf{n}) \pm \delta\pi]\!] \tag{5}$$

together produce the same Fourier intensity data on $\mathcal{L}$ as do f and μ. Then, with probability no less than $1 - |\mathcal{N}|(2\delta/\gamma)^{\lfloor S/2\rfloor}$, $\tilde{f}(\mathbf{n}) = \pm f(\mathbf{n})$ $\forall\mathbf{n}$ and furthermore $\tilde{\phi}(\mathbf{n}) = \theta + \phi(\mathbf{n})$ for a

constant $\theta \in [0, 2\pi)$ wherever $f(\mathbf{n}) \neq 0$. Here $\lfloor S/2 \rfloor$ is the greatest integer at most half the image sparsity S which is the number of nonzero pixels.

Remark 1. *If the object is known to be non-negative, then δ can be any number in $[0, 1)$ and uniqueness holds with probability no less than $1 - |\mathcal{N}|(\delta/\gamma)^{\lfloor S/2 \rfloor}$.*

For complex-valued objects uniqueness requires two independent sets of Fourier intensity data.

Theorem 2. *Let f be a complex-valued object of* rank ≥ 2. *Let the first mask $\mu^{(1)} = \mu$ in Theorem 1 with the initial mask estimate μ_0 satisfying (5).*

Suppose the second mask $\mu^{(2)}$ is exactly known and the $\mathbf{z}$-transform of $\mu^{(2)} f$ is irreducible up to a power of $\mathbf{z}^{-1}$. Moreover, assume the non-degeneracy condition that there is no $\mathbf{m} \neq \mathbf{0}$ such that $\mu^{(2)}(\mathbf{n} + \mathbf{m}) f(\mathbf{n} + \mathbf{m}) = \exp(i\xi) \exp(i\eta(\mathbf{n})) \mu^{(2)}(\mathbf{n}) f(\mathbf{n}), \forall \mathbf{n}$, and no $\mathbf{m}$ such that $\overline{\mu^{(2)}(\mathbf{m} - \mathbf{n}) f(\mathbf{m} - \mathbf{n})} = \exp(i\xi) \exp(i\eta(\mathbf{n})) \mu^{(2)}(\mathbf{n}) f(\mathbf{n}), \forall \mathbf{n}$, for some $\xi \in [0, 2\pi), |\eta(\mathbf{n})| \leq \pi\delta$. Here the over-bar notation means complex conjugacy.

Suppose that for a phase mask $\tilde{\mu}$ with (5) and an object $\tilde{f}$ the two pairs of masked objects μf and $\tilde{\mu}\tilde{f}$, $\mu^{(2)} f$ and $\mu^{(2)}\tilde{f}$, respectively, produce the same Fourier magnitudes on $\mathcal{L}$. Then with probability no less than $1 - |\mathcal{N}|(\delta/\gamma)^{\lfloor S/2 \rfloor}$ $\tilde{f}(\mathbf{n}) = \exp(i\alpha_1) f(\mathbf{n}), \forall \mathbf{n}$, and $\tilde{\mu}(\mathbf{n}) = \exp(i\alpha_2)\mu(\mathbf{n})$ if $f(\mathbf{n}) \neq 0$, where $\alpha_1, \alpha_2 \in [0, 2\pi)$.

Remark 2. *Clearly, most objects and masks obey the non-degeneracy condition.*

The proofs of Theorems 1 and 2 are given in Appendices A and B, respectively.

Both theorems assert that not only the uniqueness of the object but also the uniqueness of the mask, up to a constant phase, inside the object support. This motivates the design of our numerical schemes that turn out to be capable of enforcing uniqueness and hence nearly perfect recovery even in the presence of high uncertainty in mask phases.

3. Alternating Error Reduction (AER)

Let Λ be the diagonal matrix with diagonal elements $\{\mu(\mathbf{n})\}$ and let Φ represent the discrete Fourier transform. Denote the Fourier intensity data vector by $Y = |\Phi\Lambda f|$ where $\Lambda f(\mathbf{n}) = \mu(\mathbf{n}) f(\mathbf{n})$.

3.1. **Object Update.** Given the object estimate f_k and mask estimate μ_k at the k-th iteration, we use standard phasing algorithms to obtain f_{k+1}.

Let $\mathcal{O}$ denote the ensemble of objects $\tilde{f}$ satisfying various object constraints (see Section 7). Let $\mathcal{P}_{\mathrm{o}}$ be the orthogonal projection onto $\mathcal{O}$ (cf. [6] for details about numerical implementation of $\mathcal{P}_{\mathrm{o}}$) and $\mathcal{P}_{\mathrm{f},k} = \Lambda_k^{-1}\Phi^{-1}\mathcal{T}\Phi\Lambda_k$, where $\mathcal{T}$ is the intensity fitting operator

$$\mathcal{T}G(\boldsymbol{\omega}) = \begin{cases} Y(\boldsymbol{\omega}) \exp(i\measuredangle G(\boldsymbol{\omega})) & \text{if } |G(\boldsymbol{\omega})| > 0 \\ Y(\boldsymbol{\omega}) & \text{if } |G(\boldsymbol{\omega})| = 0 \end{cases}. \tag{6}$$

Here and below $\measuredangle z \in [0, 2\pi)$ denotes the wrapped phase angle of z. When $z = 0$, $\measuredangle z$ is taken to be 0 unless specified otherwise.

Error Reduction (ER) takes the form $f_{k+1} = \mathcal{P}_{\mathrm{o}}\mathcal{P}_{\mathrm{f},k} f_k$ which can be conveniently represented by the diagram in Figure 1(a).

Let $r(\tilde{f}, \tilde{\mu}) = \| \, |\Phi\tilde{\Lambda}\tilde{f}| - Y \, \|$ denote the residual. Here and below $\| \cdot \|$ stands for the Euclidean norm. With a phase mask, ER enjoys the residual reduction property [6, 8]:

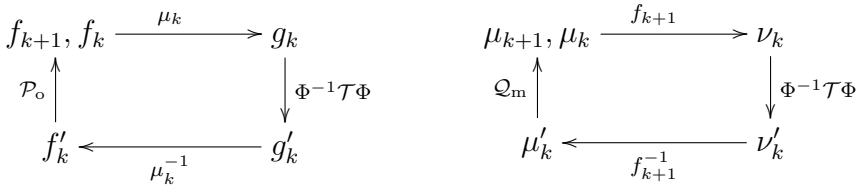

(a) object update (b) mask update

FIGURE 1. Alternating Error Reduction (AER) between object and mask.

$$r(f_{k+1}, \mu_k) \le r(f_k, \mu_k). \tag{7}$$

3.2. **Mask Update.** Based on the newly updated object estimate f_{k+1}, we define $\mathcal{Q}_{\mathrm{f},k}$ as

$$\mu'_k = \mathcal{Q}_{\mathrm{f},k}\mu_k(\mathbf{n}) = \begin{cases} \Phi^{-1}\mathcal{T}\Phi\Lambda_k f_{k+1}(\mathbf{n})/f_{k+1}(\mathbf{n}) & \text{if } f_{k+1}(\mathbf{n}) \neq 0 \\ \\ \mu_k(\mathbf{n}) & \text{else} \end{cases}. \tag{8}$$

Let $\mathcal{M}$ be the ensemble of phase masks satisfying the phase uncertainty constraint (5):

$$\mathcal{M} \;=\; \{\tilde{\mu} \mid \forall \mathbf{n}, |\tilde{\mu}(\mathbf{n})| = 1 \text{ and } \measuredangle\tilde{\mu}(\mathbf{n}) \in [\![\phi_0(\mathbf{n}) \pm \delta\pi]\!]\}. \tag{9}$$

Let $\mathcal{Q}_{\mathrm{m}}$ be the orthogonal projection onto $\mathcal{M}$. Note that $\mathcal{Q}_{\mathrm{m}}$ can be computed pixel by pixel as follows.

Let $a = (\phi_0(\mathbf{n}) - \delta\pi) (\mathrm{mod}\ 2\pi)$, $b = (\phi_0(\mathbf{n}) + \delta\pi) (\mathrm{mod}\ 2\pi)$ and

$$c = \begin{cases} \pi + (a+b)/2\,(\mathrm{mod}\,2\pi), & \text{if } \ a \le b \\ (a+b)/2\,(\mathrm{mod}\,2\pi), & \text{else.} \end{cases}$$

Then $\mathcal{Q}_{\mathrm{m}}$ can be expressed as

$$\mathcal{Q}_{\mathrm{m}}\mu'_k(\mathbf{n}) = \begin{cases} \exp\left(i\measuredangle\mu'_k(\mathbf{n})\right) & \text{if } \measuredangle\mu'_k(\mathbf{n}) \in [\![a, b]\!] \\ \exp\left(ib\right) & \text{if } \measuredangle\mu'_k(\mathbf{n}) \in [\![b, c]\!] \\ \exp\left(ia\right) & \text{if } \measuredangle\mu'_k(\mathbf{n}) \in [\![c, a]\!]. \end{cases} \tag{10}$$

Since the the object and the mask have interchangeable roles, we set $\mu_{k+1} = \mathcal{Q}_{\mathrm{m}}\mathcal{Q}_{\mathrm{f},k}\mu_k$ in the spirit of ER (see Fig. 1(b)). Note the differences between the mask update rule here and that of the extended ptychographical engine (ePIE) ((4) in [15]): First, (8) uses the newly updated object f_{k+1} while ePIE uses the previous one. Second, more importantly, the rough prior knowledge about the mask is enforced by $\mathcal{Q}_{\mathrm{m}}$ here while ePIE does not consider this aspect.

Now we prove the following residual reduction property.

Lemma 1. *With $\mathcal{Q}_{\mathrm{m}}$ we have*

$$r(f_{k+1}, \mu_{k+1}) \le r(f_{k+1}, \mu_k)$$

The proof of Lemma 1 is given in Appendix C.

Define the Alternating Error Reduction (AER) as

$$(f_{k+1}, \mu_{k+1}) \;=\; (\mathcal{P}_{\mathrm{o}}\mathcal{P}_{\mathrm{f},k}f_k, \mathcal{Q}_{\mathrm{m}}\mathcal{Q}_{\mathrm{f},k}\mu_k). \tag{11}$$

In words, AER alternates between updating the object and the mask estimates until the iteration converges.

Lemma 1 and (7) together yield the following residual reduction property for AER.

Theorem 3. *AER (11) has the residual reduction property:* $r(f_{k+1}, \mu_{k+1}) \leq r(f_k, \mu_k)$.

In our numerical tests, we find that while $\mathcal{Q}_{\rm m}$ works well for real-valued objects, for complex-valued objects the following alternative rule works better

$$\hat{\mathcal{Q}}_{\rm m}\mu'_k(\mathbf{n}) = \begin{cases} \exp\left(i\measuredangle\mu'_k(\mathbf{n})\right) & \text{if } \measuredangle\mu'_k(\mathbf{n}) \in [\![a, b]\!] \\ \mu_0(\mathbf{n}), & \text{else} \end{cases} \tag{12}$$

where μ_0 is the initial mask estimate. With $\hat{\mathcal{Q}}_{\rm m}$ we have the alternative version of AER

$$(f_{k+1}, \mu_{k+1}) \;=\; (\mathcal{P}_{\rm o}\mathcal{P}_{{\rm f},k}f_k, \hat{\mathcal{Q}}_{\rm m}\mathcal{Q}_{{\rm f},k}\mu_k). \tag{13}$$

4. Alternating Douglas-Rachford and Error-Reduction (DRER)

AER (either version) by itself converges slowly, typically taking up to several thousands steps for accurate recovery in our numerical tests. To speed up convergence we consider the Douglas-Rachford (DR) algorithm [4, 14], also called the averaged alternating reflections [2], which coincides with the hybrid input-output (HIO) algorithm for the parameter $\beta = 1$ when object value constraints are not imposed [1]

$$f_{k+1} = \frac{I + \mathcal{R}_{\rm o}\mathcal{R}_{{\rm f},k}}{2} f_k \tag{14}$$

where $\mathcal{R}_{\rm o} = 2\mathcal{P}_{\rm o} - I, \quad \mathcal{R}_{{\rm f},k} = 2\mathcal{P}_{{\rm f},k} - I$ are reflection operators.

Define the DRER iteration as

$$(f_{k+1}, \mu_{k+1}) \;=\; \left(\frac{1}{2}(I + \mathcal{R}_{\rm o}\mathcal{R}_{{\rm f},k})f_k, \mathcal{Q}_{\rm m}\mathcal{Q}_{{\rm f},k}\mu_k\right) \tag{15}$$

and the alternative version as

$$(f_{k+1}, \mu_{k+1}) \;=\; \left(\frac{1}{2}(I + \mathcal{R}_{\rm o}\mathcal{R}_{{\rm f},k})f_k, \hat{\mathcal{Q}}_{\rm m}\mathcal{Q}_{{\rm f},k}\mu_k\right). \tag{16}$$

To strictly enforce the mask constraint, we do not use DR for mask update.

5. AER/DRER with two sets of data

Let $\mu^{(1)} = \mu$ and $\mu^{(2)}$ be two masks with which two sets of Fourier intensity data $Y = |\Phi\Lambda f|$ and $Y^{(2)} = |\Phi\Lambda^{(2)} f|$ are measured on $\mathcal{L}$. Let $\mathcal{T}$ and $\mathcal{T}^{(2)}$ be the intensity fitting operators corresponding to Y and $Y^{(2)}$, respectively.

For simplicity of presentation we assume the second mask (random or deterministic) is exactly known and independent from the first mask which is random. In this case, there is no need for the second mask update.

Suppose f_k and μ_k are the image and the mask recovered at the end of the k-th iteration. At the $(k+1)$-st iteration, the image is first updated from f_k to f_{k+1} based on μ_k and $\mu^{(2)}$. Let $\mathcal{P}_k = \Lambda_k^{-1}\Phi^{-1}\mathcal{T}\Phi\Lambda_k$ and $\mathcal{P}^{(2)} = (\Lambda^{(2)})^{-1}\Phi^{-1}\mathcal{T}^{(2)}\Phi\Lambda^{(2)}$.

The AER and DRER algorithms with two masks are respectively

$$(f_{k+1}, \mu_{k+1}) = \left(\mathcal{P}_{\mathrm{o}}\mathcal{P}^{(2)}\mathcal{P}_k f_k, \mathcal{Q}_m \mathcal{Q}_{\mathrm{f},k}\mu_k\right), \quad k = 0, 1, \cdots \tag{17}$$

$$(f_{k+1}, \mu_{k+1}) = \left(\frac{1}{2}(I + \mathcal{R}_{\mathrm{o}}(2\mathcal{P}^{(2)}\mathcal{P}_k - I))f_k, \mathcal{Q}_m \mathcal{Q}_{\mathrm{f},k}\mu_k\right). \tag{18}$$

The following alternative versions work better for complex-valued objects:

$$(f_{k+1}, \mu_{k+1}) = \left(\mathcal{P}_{\mathrm{o}}\mathcal{P}^{(2)}\mathcal{P}_k f_k, \hat{\mathcal{Q}}_{\mathrm{m}} \mathcal{Q}_{\mathrm{f},k}\mu_k\right), \quad k = 0, 1, \cdots \tag{19}$$

$$(f_{k+1}, \mu_{k+1}) = \left(\frac{1}{2}(I + \mathcal{R}_{\mathrm{o}}(2\mathcal{P}^{(2)}\mathcal{P}_k - I))f_k, \hat{\mathcal{Q}}_{\mathrm{m}} \mathcal{Q}_{\mathrm{f},k}\mu_k\right) \tag{20}$$

6. Extension to general masks

The preceding discussion is limited to the case of phase masks. It is easy to extend the above results to general masks, if the mask intensities are certain (i.e. exactly known) and strictly positive, as follows.

Let the mask be rewritten as $\mu(\mathbf{n}) = |\mu|(\mathbf{n}) \exp(i\phi(\mathbf{n}))$, with $|\mu(\mathbf{n})| > 0, \forall \mathbf{n} \in \mathcal{N}$, where $|\mu|$ is certain and ϕ is uncertain as before. Define the auxiliary object $\tilde{f}(\mathbf{n}) = f(\mathbf{n})|\mu|(\mathbf{n})$. The Fourier phasing problem for the object f and the mask μ is equivalent to that for the auxiliary object $\tilde{f}$ and the phase mask $\exp(i\phi)$ which can be solved as above. The original object can then be recovered by dividing the recovered auxiliary object by the known, nonzero mask intensities $|\mu|$.

In this extension, any uncertainty of the mask intensities is converted into that of the object. So in case that $|\mu|$ is unknown or highly uncertain our approach needs substantial modification to proceed unless the object intensities are known *a priori*. For example, if the object is a phase object ($|f| = 1$) then we can proceed as if the object were $\tilde{f} = f|\mu|$ and the mask were $\exp(i\phi)$. After the auxiliary object is recovered, the phase object can be recovered by normalization.

7. Numerical Simulations

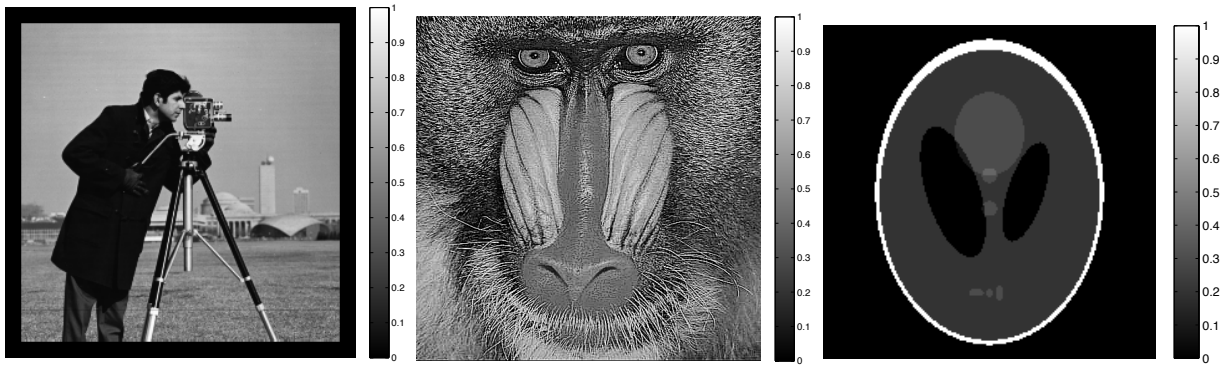

(a) 282×282 cameraman (b) 512×512 mandrill (c) 200×200 phantom

Figure 2. Test images of loose support (a)(c) and tight support (b)

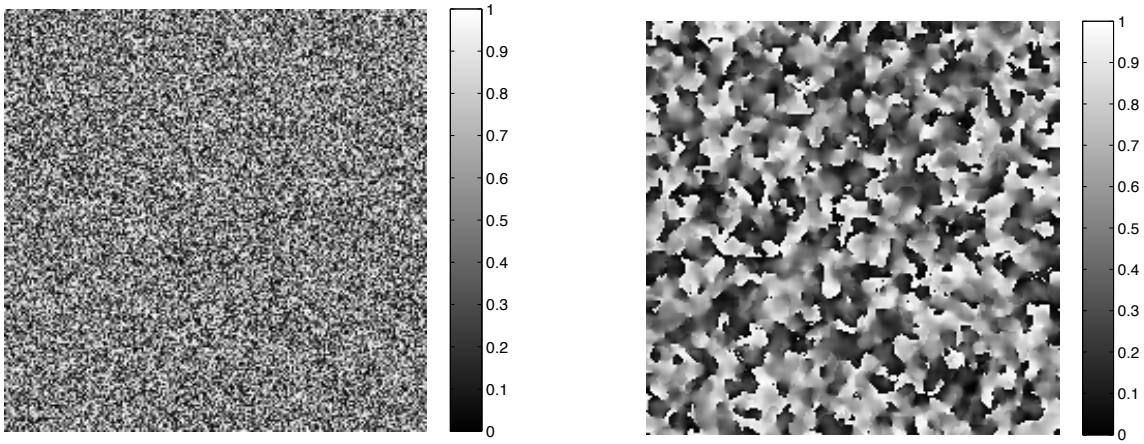

(a) HRM (b) LRM

FIGURE 3. (a) HRM and (b) LRM. The gray scale represents the phase range $[0, 1]$ in the unit of 2π.

In this section, we test our numerical schemes by performing phasing with a PUM.

The original images are the 256×256 cameraman, the 138×184 phantom and the 512×512 mandrll (Fig.2(c)). We surround the first two images by dark (i.e. zero-valued) borders to create the 282×282 cameraman and the 200×200 phantom of loose supports (Fig. 2(a)&(b)). Objects of loose support are harder to recover than the same objects of tight support (without zero-padding).

First we consider the case with $\gamma = 1$. Let $\{\phi_0(\mathbf{n})\}$ and $\{\psi(\mathbf{n})\}$ be two independent sets of independent uniform random variables over $[-\pi, \pi)$. Define the mask phases $\phi(\mathbf{n}) = \phi_0(\mathbf{n}) + \delta\psi(\mathbf{n})$. We refer to the corresponding mask $\mu = \exp[i\phi]$ as a full-ranged *high resolution* mask (HRM), Fig. 3(a).

To demonstrate that the random mask approach is stable with respect to the correlation length of the mask, we define a full-ranged *low resolution* mask (LRM) as follows. Let $\{\tilde{\phi}_0(\mathbf{n})\}$ and $\{\tilde{\psi}(\mathbf{n})\}$ be two independent sets of independent uniform random variables over $[-\pi, \pi)$.

Convolving $\exp(i\tilde{\phi}_0)$ with the kernel function

$$g_c(\mathbf{x}) = \begin{cases} \exp[-c^2/(c^2 - |\mathbf{x}|^2)], & |\mathbf{x}| \le c \\ 0, & \text{else} \end{cases}$$

with $c = 5$ and normalizing the outcome to have modulus one we obtain the LRM estimate $\mu_0 = \exp[i\phi_0]$, Fig. 3(b). Repeating the same procedure with $\exp[i\tilde{\psi}]$ we obtain $\exp[i\psi]$. We then set the LRM $\mu = \exp(i\phi)$ with phase $\phi = \phi_0 + \delta\psi$. The resulting mask phases and their estimates are uniform random variables over $[-\pi, \pi)$ with a correlation length of about 10 pixel sizes and hence have much lower (100 times less) degrees of diversity than HRM. Consequently HRM tends to yield a better perform in recovery than LRM (cf. Fig. 8).

When a second set of Fourier data is used (for complex-valued objects), the data are synthesized with a UM (i.e. $\mu^{(2)} = 1$).

A standard way to utilize the oversampled data for $\sigma > 1$ is to enlarge the original image by adding corresponding number of zero pixels which is then enforced as an additional object constraint. This procedure is called the oversampling method [18] and implemented in all our simulations with $\sigma = 4$.

7.1. **Error and Residual.** To estimate the recovery, we define relative error and relative residual as follows. Let $\hat{f}$ and $\hat{\mu}$ be the recovered image and mask respectively. The relative error of reconstruction is defined as

$$e(\hat{f}) = \begin{cases} \|f - \hat{f}\|/\|f\| & \text{if absolute uniqueness holds} \\ \min\limits_{\alpha\in[0,2\pi)} \|f - \exp(i\alpha)\hat{f}\|/\|f\| & \text{if uniqueness holds only up to a global phase} \end{cases}.$$

Let $\hat{\Lambda}$ be the diagonal matrix whose diagonal elements are $\hat{\mu}(\mathbf{n})$. The relative residual is defined as

$$\rho(\hat{f}, \hat{\mu}) = \frac{\| \ Y - |\Phi\hat{\Lambda}\mathcal{P}_{\rm o}\hat{f}| \ \|}{\|Y\|}$$

where $\mathcal{P}_{\rm o}$ is introduced to enforce the object constraints in the case of DRER.

7.2. **Performance study of AER and DRER.** First we use AER (11) to recover the non-negative images with the stopping rule $\|f_{k+1} - f_k\|/\|f_k\| < 0.05\%$ and one LRM of uncertainty $\delta = 0.3$. The results, shown in Fig. 4, are noisy and inaccurate with 36.56% error for the cameraman, 59.50% error for the phantom and 44.28% for the mandrill. Consistent with the residual reduction property (Theorem 3), the residual curves in Fig. 4 are monotonically decreasing.

Much improvement can be gained by running DRER, followed by AER. For real-valued objects, we use the version of DRER (15). DRER (15) is stopped when $\|f_{k+1} - f_k\|/\|f_k\| < 1\%$, with the maximum of 500 steps, and AER (11) is terminated when $\|f_{k+1} - f_k\|/\|f_k\| < 0.05\%$, with the maximum of 500 steps. As shown in Figure 5, the results are 90 DRER and 6 AER steps with 1.26% error for the cameraman, 72 DRER and 5 AER with 0.37% error for the phantom and 61 DRER and 6 AER with 0.96% error for the mandrill. Consistent with Theorem 1, the mask errors occur only outside the object supports.

Next we consider the case of the complex-valued objects without phase constraint and with one UM and one LRM of uncertainty $\delta = 0.3$. We apply the alternative versions of DRER (20) and AER (19) which tend to produce better results than (15) and (11) for complex-valued objects. DRER (20) is stopped when $\|f_{k+1} - f_k\|/\|f_k\| < 1\%$, with the maximum of 500 steps, and AER (19) is terminated when $\|f_{k+1} - f_k\|/\|f_k\| < 0.05\%$, with the maximum of 500 steps. Fig. 6 shows the results for object phases randomly distributed on $[0, 2\pi)$. Both algorithms ran their full course of 500 steps with 6.43% error for the cameraman, 2.20% error for the phantom and 4.62% for the mandrill. The mask errors occur only outside the object supports, consistent with Theorem 2.

Still next, we consider complex images with the $\pi/2$-sector constraint that the object phases are randomly distributed in $[0, \pi/2]$. In the setting of X-ray diffractive imaging the real part represents the effective density of coherently diffracting electrons and the imaginary

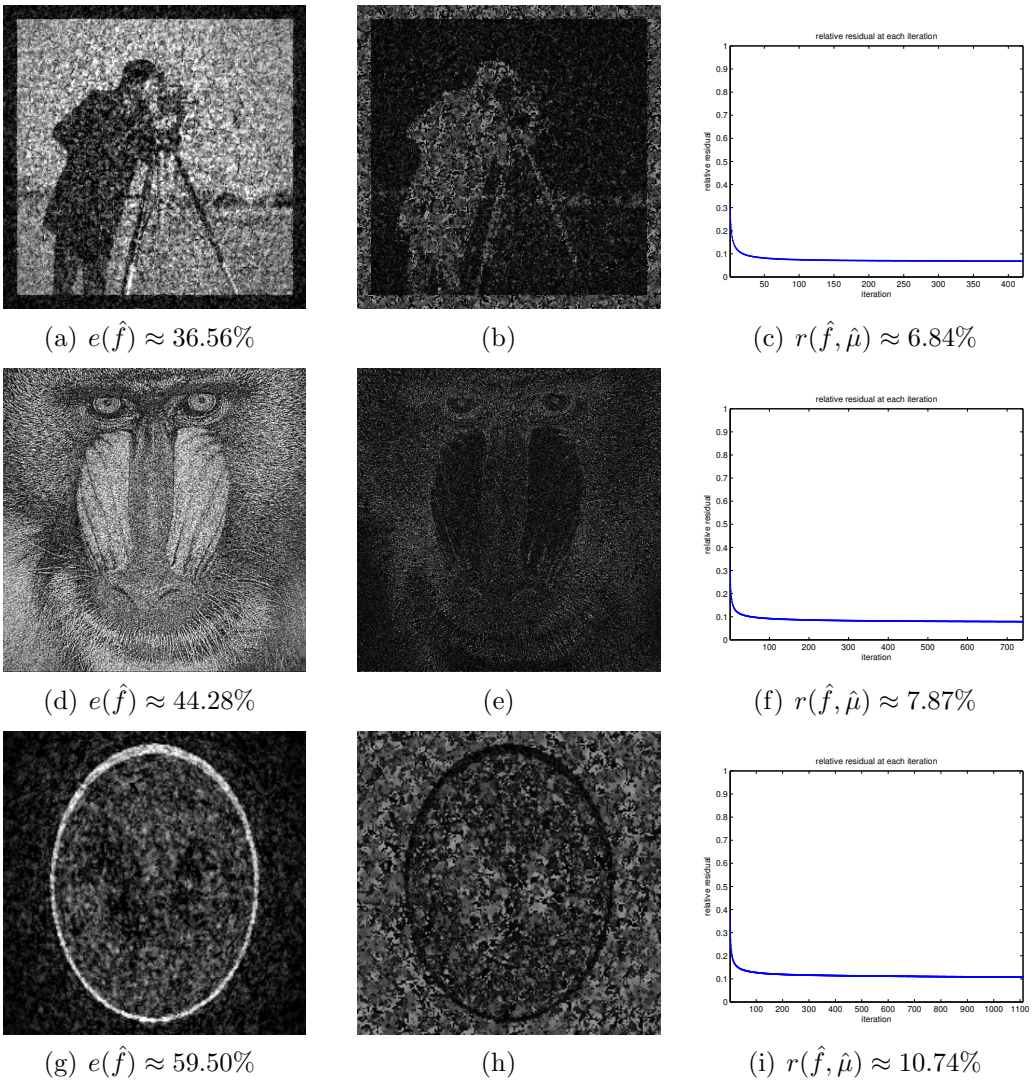

(a) $e(\hat{f}) \approx 36.56\%$ (b) (c) $r(\hat{f}, \hat{\mu}) \approx 6.84\%$

(d) $e(\hat{f}) \approx 44.28\%$ (e) (f) $r(\hat{f}, \hat{\mu}) \approx 7.87\%$

(g) $e(\hat{f}) \approx 59.50\%$ (h) (i) $r(\hat{f}, \hat{\mu}) \approx 10.74\%$

FIGURE 4. Recovery of non-negative images by AER with one LRM of $\delta = 0.3$. The middle column shows the absolute phase differences between μ and $\hat{\mu}$. The right column shows the relative residual at each iteration.

part represents the attenuation effect, so both of them are usually positive [19]. With the sector constraint, we found that the following stopping rule can significantly reduce the number of iterations: DRER (20) is stopped if the residual increases in five consecutive steps, with the maximum of 500 steps, and AER (19) is terminated when $\|f_{k+1} - f_k\|/\|f_k\| < 0.05\%$, with the maximum of 500 steps. Fig. 7 shows the results with one UM and one LRM of uncertainty $\delta = 0.3$. With the new stopping rule and the sector constraint, 21 DRER and 500 AER steps took place with 2.62% error for the cameraman, 23 DRER and 500 AER steps with 1.47 % error for the phantom and 23 DRER and 500 AER steps with 2.16% for the mandrill.

Fig. 8 shows the averaged relative error $e(\hat{f})$, after 5 runs of independently chosen initial guesses for the object, with or without mask update, as a function of the mask uncertainty

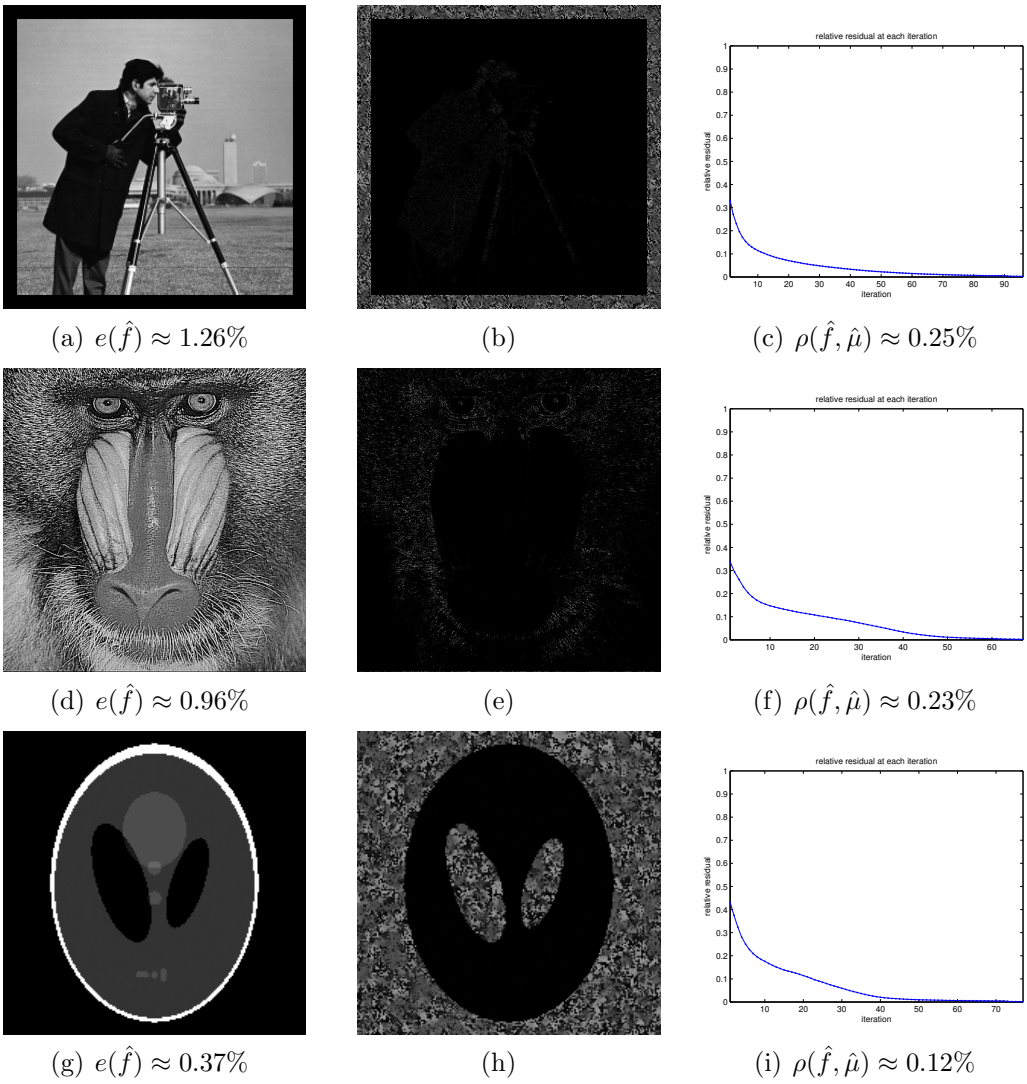

(a) $e(\hat{f}) \approx 1.26\%$ (b) (c) $\rho(\hat{f}, \hat{\mu}) \approx 0.25\%$

(d) $e(\hat{f}) \approx 0.96\%$ (e) (f) $\rho(\hat{f}, \hat{\mu}) \approx 0.23\%$

(g) $e(\hat{f}) \approx 0.37\%$ (h) (i) $\rho(\hat{f}, \hat{\mu}) \approx 0.12\%$

FIGURE 5. Recovery of non-negative images with one LRM of $\delta = 0.3$. (a) the recovered cameraman $\hat{f}$ by 90 DRER + 6 AER steps. (d) the recovered mandrill $\hat{f}$ by 61 DRER + 6 AER steps. (g) the recovered phantom $\hat{f}$ by 72 DRER + 5 AER steps. The middle column shows the absolute phase differences between μ and $\hat{\mu}$. The right column shows the relative residual at each iteration.

of HRM or LRM for non-negative images (a)(d)(g), complex-valued images under the $\pi/2$-section condition (b)(e)(h) and complex-valued images images with totally random phases (c)(f)(i). We use the same stopping rules and updating rules as above for each case, except that the maximum number of steps is changed to $200+\delta \cdot 1000$ for DRER and AER separately to deal with variable uncertainty.

Without mask update the error curves are roughly linear with the noise amplification factor roughly 2 (blue and black curves), consistent with our previous results reported in [6]. With mask update, the results (pink and red curves) are drastically improved in all cases.

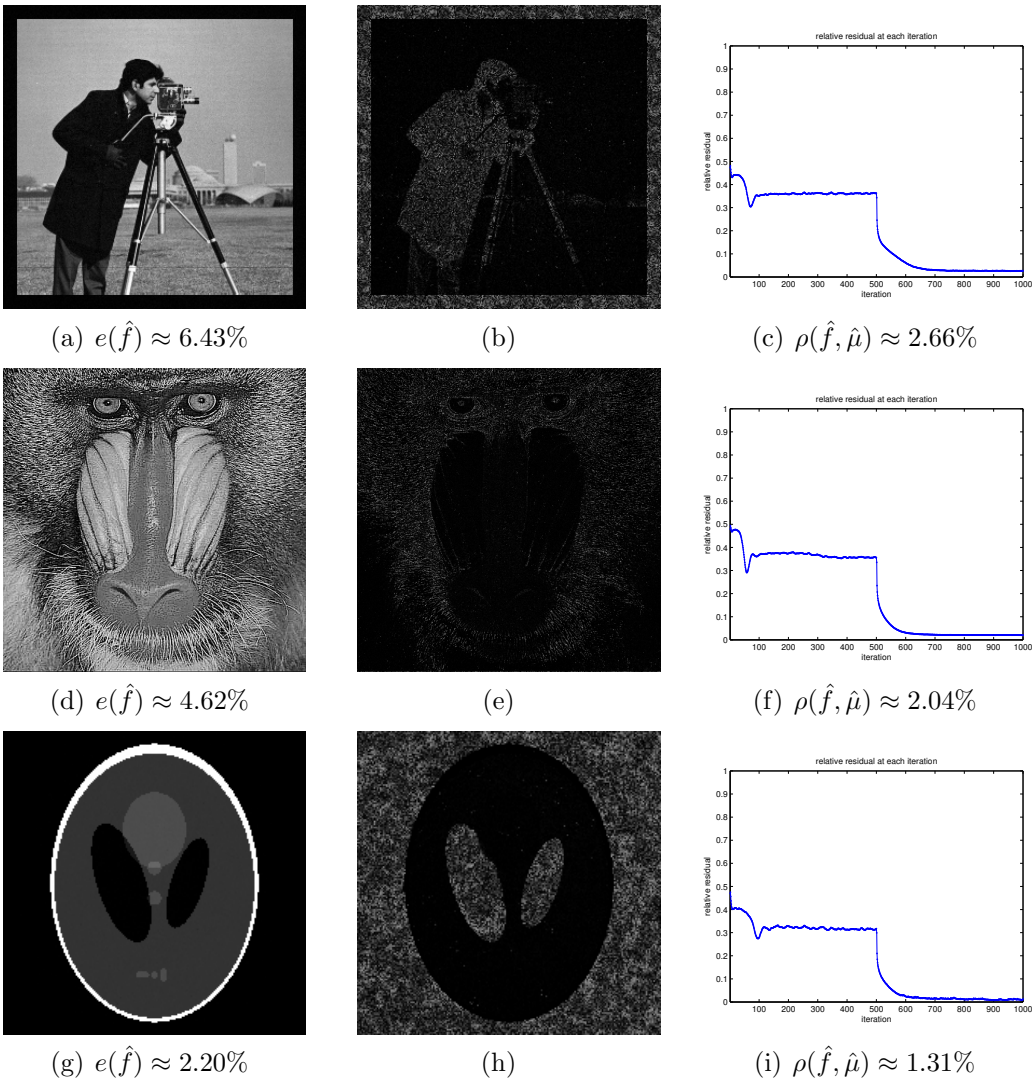

(a) $e(\hat{f}) \approx 6.43\%$ (b) (c) $\rho(\hat{f}, \hat{\mu}) \approx 2.66\%$

(d) $e(\hat{f}) \approx 4.62\%$ (e) (f) $\rho(\hat{f}, \hat{\mu}) \approx 2.04\%$

(g) $e(\hat{f}) \approx 2.20\%$ (h) (i) $\rho(\hat{f}, \hat{\mu}) \approx 1.31\%$

FIGURE 6. Recovery of unconstrained complex-valued images with one UM and one LRM of $\delta = 0.3$. (a) absolute values of the recovered cameraman $\hat{f}$ by 500 DRER + 500 AER steps. (d) absolute values of the recovered mandrill $\hat{f}$ by 500 DRER + 500 AER steps. (g) absolute values of the recovered phantom $\hat{f}$ by 500 DRER + 500 AER steps. The middle column shows the absolute phase differences between μ and $\hat{\mu}$. The right column shows the relative residual at each iteration.

Fig. 9 shows the relative error versus the range of mask phases. Consistent with the lower bound for uniqueness probability $1 - |\mathcal{N}|(\delta/\gamma)^{\lfloor S/2 \rfloor}$ in Theorems 1 and 2, the error starts to drop precipitously around $\gamma \approx 0.3$. The recovery of the mandrill has the best performance near the threshold $\gamma \approx \delta$ probably because it has the highest sparsity S among the tested images. It is also surprising that the nonnegative mandrill image can be accurately recovered with γ slightly greater than 0.2 (Fig. 9(a)).

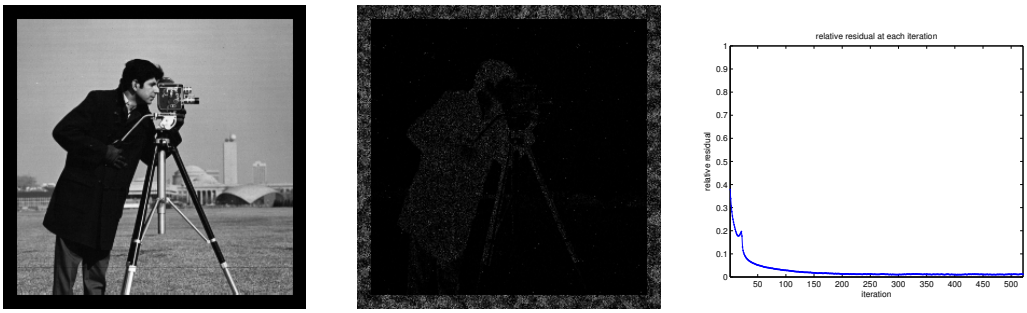

(a) $e(\hat{f}) \approx 2.62\%$ (b) (c) $\rho(\hat{f}, \hat{\mu}) \approx 1.12\%$

(d) $e(\hat{f}) \approx 2.16\%$ (e) (f) $\rho(\hat{f}, \hat{\mu}) \approx 1.03\%$

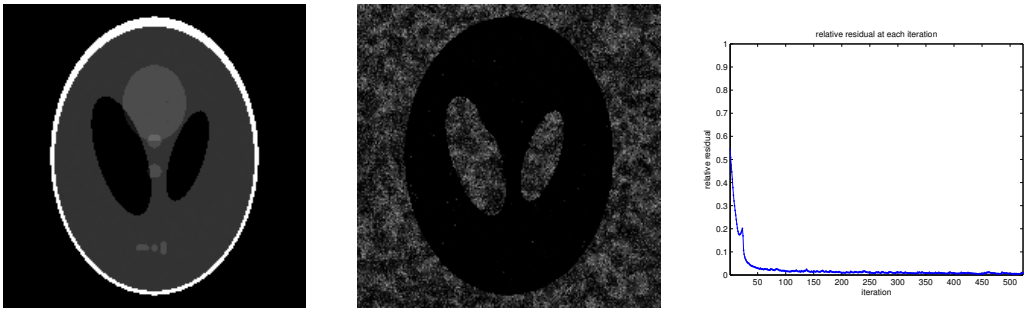

(g) $e(\hat{f}) \approx 1.47\%$ (h) (i) $\rho(\hat{f}, \hat{\mu}) \approx 0.80\%$

FIGURE 7. Recovery of the $\pi/2$-sector constrained images with one UM and one LRM of $\delta = 0.3$. (a) absolute values of the recovered cameraman $\hat{f}$ by 21 DRER + 500 AER steps. (d) absolute values of the recovered mandrill $\hat{f}$ by 23 DRER + 500 AER steps. (g) absolute values of the recovered phantom $\hat{f}$ by 23 DRER + 500 AER steps. The middle column shows the absolute phase differences between μ and $\hat{\mu}$. The right column shows the relative residual at each iteration.

8. Conclusion

We proved the uniqueness, up to a global phase, for phasing with PUM with probability exponentially close to one, depending on the object sparsity and mask uncertainty. We designed algorithms that achieve nearly perfect recovery for mask uncertainty up to half of that promised by the uniqueness results. Additional object constraint such as the sector condition increases the degree of uncertainty in the mask that can be dealt with by our algorithms.

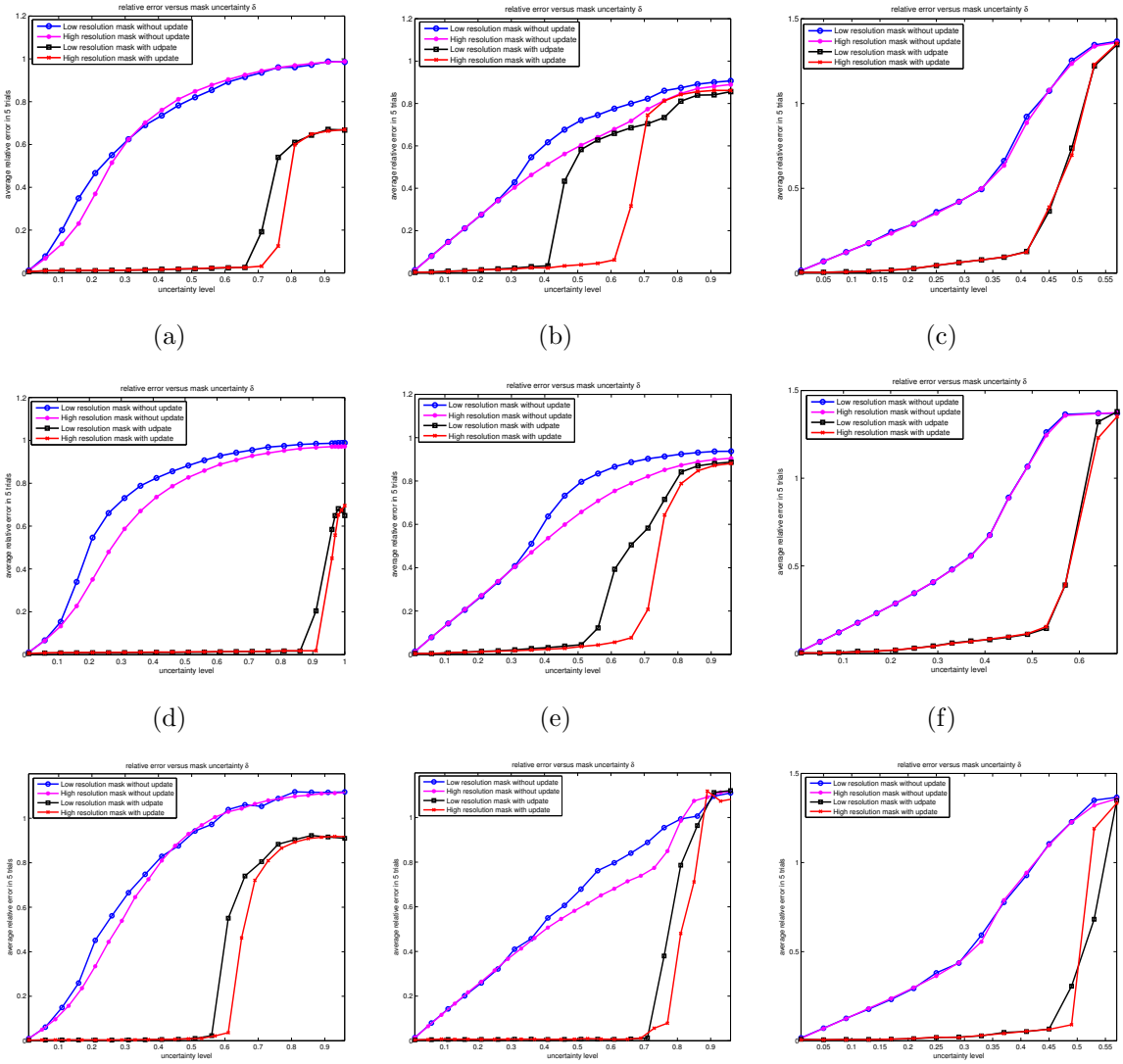

FIGURE 8. Averaged relative error $e(\hat{f})$ of 5 independent runs versus the percentage of mask uncertainty for nonnegative images (left column), $\pi/2$-sector images (middle column) and unconstrained images in the order of cameraman, mandrill and phantom (top to bottom). The stopping rules and mask updating rules are the same as described in the main text for each case with the maximum of $200 + 1000 \cdot \delta$ steps for DRER and AER separately.

As a by-product of object recovery the unknown mask can be recovered accurately within the object support. The numerical performance is robust with respect to the correlation in the mask as well as various types of noises as shown in the previous study [6]. An important parameter controlling the performance of our methods is the diversity of the mask phases.

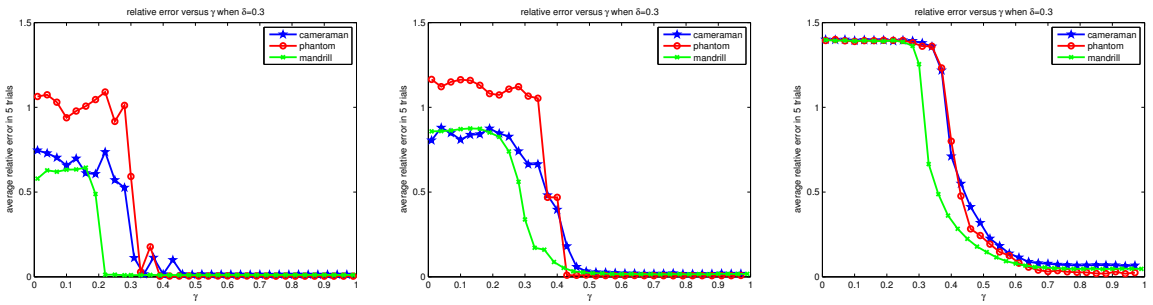

(a) Nonnegative images (b) $\pi/2$-sector images (c) Unconstrained images

FIGURE 9. Relative error versus the mask phase range γ for (a) nonnegative, (b) $\pi/2$-sector and (c) unconstrained images with $\delta = 0.3$.

Our method can be easily extended to general masks with phase and amplitude modulation if the mask amplitudes are known exactly. If the mask amplitudes are also uncertain, the proposed method will have to be substantially modified. This will be a topic of future study.

APPENDIX A. PROOF OF THEOREM 1

Proof. In view of Proposition 1, there exist some $\mathbf{m}$ and $\theta \in [0, 2\pi)$ such that either

$$\tilde{\mu}(\mathbf{n})\tilde{f}(\mathbf{n}) = \exp(i\theta)\mu(\mathbf{m}+\mathbf{n})f(\mathbf{m}+\mathbf{n}) \tag{21}$$

or

$$\tilde{\mu}(\mathbf{n})\tilde{f}(\mathbf{n}) = \exp(i\theta)\overline{\mu(\mathbf{m}-\mathbf{n})f(\mathbf{m}-\mathbf{n})}. \tag{22}$$

In the case of (21) with any $\mathbf{m} \neq \mathbf{0}$ and any $\theta \in [0, 2\pi)$,

$$\tilde{f}(\mathbf{n}) = \exp(i\theta)\frac{|\mu(\mathbf{m}+\mathbf{n})|\exp(i\phi(\mathbf{n}+\mathbf{m}))}{|\tilde{\mu}(\mathbf{n})|\exp(i\measuredangle\tilde{\mu}(\mathbf{n}))}f(\mathbf{n}+\mathbf{m}).$$

Consider the $\lfloor S/2 \rfloor$ independently distributed r.v.s. of $\mu(\mathbf{n}+\mathbf{m})$ where $f(\mathbf{n}+\mathbf{m}) \neq 0$ corresponding to $\lfloor S/2 \rfloor$ nonoverlapping pairs of points $\{\mathbf{n}, \mathbf{n}+\mathbf{m}\}$. For every $\mathbf{n}$ where $f(\mathbf{n}+\mathbf{m}) \neq \mathbf{0}$, a proper choice of $\measuredangle\tilde{\mu}(\mathbf{n})$ makes $\tilde{f}(\mathbf{n})$ real-valued if and only if either

$$\phi(\mathbf{n}+\mathbf{m}) \in [\![\phi_0(\mathbf{n}) - \theta - \measuredangle f(\mathbf{n}+\mathbf{m}) \pm \delta\pi]\!]$$

or

$$\phi(\mathbf{n}+\mathbf{m}) \in [\![(\phi_0(\mathbf{n}) - \theta - \measuredangle f(\mathbf{n}+\mathbf{m}) + \pi) \pm \delta\pi]\!]$$

However, $\phi(\mathbf{n}+\mathbf{m})$ is independently and uniformly distributed in $[-\gamma\pi, \gamma\pi]$, so it falls in these two regions with probability at most $2\delta/\gamma$. The probability for every such $\tilde{f}(\mathbf{n})$ to be real-valued is at most $2\delta/\gamma$ and hence the probability for all $\tilde{f}(\mathbf{n})$ with $\mathbf{m} \neq 0$ to be real-valued is at most $(2\delta/\gamma)^{\lfloor S/2 \rfloor}$.

The union over $\mathbf{m} \neq 0$ of these events has probability at most $|\mathcal{N}|(2\delta)^{\lfloor S/2 \rfloor}$. Therefore, with probability at least $1 - |\mathcal{N}|(2\delta)^{\lfloor S/2 \rfloor}$, $\mathbf{m} = \mathbf{0}$ and $\exp(i\theta)\mu(\mathbf{n})f(\mathbf{n}) = \tilde{\mu}(\mathbf{n})\tilde{f}(\mathbf{n})$ $\forall \mathbf{n}$ which further implies that $\tilde{f}(\mathbf{n}) = \pm f(\mathbf{n})$ $\forall \mathbf{n}$ and $\tilde{\mu}(\mathbf{n}) = \pm\exp(i\theta)\mu(\mathbf{n})$ on $\mathbf{n}$ where $f(\mathbf{n}) \neq 0$.

Likewise the probability for all $\tilde{f}(\mathbf{n})$ given by (22) to be real-valued for any $\mathbf{m}$ is at most $|\mathcal{N}|(2\delta)^{\lfloor S/2 \rfloor}$. □

Appendix B. Proof of Theorem 2

Proof. In view of Proposition 1, for some $\mathbf{m}_1, \mathbf{m}_2$ and $\theta_1, \theta_2 \in [0, 2\pi)$ either

$$\exp(i\theta_1)\mu(\mathbf{n}+\mathbf{m}_1)f(\mathbf{n}+\mathbf{m}_1) = \tilde{\mu}(\mathbf{n})\tilde{f}(\mathbf{n}) \tag{23}$$

or

$$\exp(i\theta_1)\overline{\mu(\mathbf{m}_1-\mathbf{n})f(\mathbf{m}_1-\mathbf{n})} = \tilde{\mu}(\mathbf{n})\tilde{f}(\mathbf{n}) \tag{24}$$

as well as

$$\exp(i\theta_2)\mu^{(2)}(\mathbf{n}+\mathbf{m}_2)f(\mathbf{n}+\mathbf{m}_2) = \mu^{(2)}(\mathbf{n})\tilde{f}(\mathbf{n}) \tag{25}$$

or

$$\exp(i\theta_2)\overline{\mu^{(2)}(\mathbf{m}_2-\mathbf{n})f(\mathbf{m}_2-\mathbf{n})} = \mu^{(2)}(\mathbf{n})\tilde{f}(\mathbf{n}). \tag{26}$$

There are four possible combinations of (23), (24), (25) and (26).

In the case of (23)&(25), we have

$$\exp(i\theta_1)\mu(\mathbf{n}+\mathbf{m}_1)\mu^{(2)}(\mathbf{n})f(\mathbf{n}+\mathbf{m}_1) = \exp(i\theta_2)\mu^{(2)}(\mathbf{n}+\mathbf{m}_2)\tilde{\mu}(\mathbf{n})f(\mathbf{n}+\mathbf{m}_2). \tag{27}$$

For any $\mathbf{m}_1 \neq \mathbf{0}$ and any $\theta_1, \theta_2 \in [0, 2\pi)$, consider the $\lfloor S/2 \rfloor$ pairs of independently distributed r.v.s. of $\mu(\mathbf{n}+\mathbf{m}_1)$ where $f(\mathbf{n}+\mathbf{m}_1) \neq 0$ corresponding to $\lfloor S/2 \rfloor$ non overlapping sets of points $\{\mathbf{n}, \mathbf{n}+\mathbf{m}_1\}$. For every $\mathbf{n}$, a proper choice of $\tilde{\mu}(\mathbf{n})$ makes (27) true if and only if

$$\begin{aligned} &\phi(\mathbf{n}+\mathbf{m}_1) \\ &\in \ [\![(\phi_0(\mathbf{n}) + \theta_2 - \theta_1 + \phi^{(2)}(\mathbf{n}+\mathbf{m}_2) - \phi^{(2)}(\mathbf{n}) + \measuredangle f(\mathbf{n}+\mathbf{m}_2) - \measuredangle f(\mathbf{n}+\mathbf{m}_1)) \pm \delta\pi]\!] \end{aligned} \tag{28}$$

where $\phi^{(2)}(\mathbf{n}) = \measuredangle \mu^{(2)}(\mathbf{n})$.

Since $\phi(\mathbf{n}+\mathbf{m}_1)$ are independently and uniformly distributed in $[-\gamma\pi, \gamma\pi]$, (28) holds for each $\mathbf{n}$ with probability at most δ/γ and hence (27) holds for all $\mathbf{n}$ at once with probability at most $(\delta/\gamma)^{\lfloor S/2 \rfloor}$.

The union over $\mathbf{m}_1 \neq \mathbf{0}$ of these events has probability at most $|\mathcal{N}|(\delta/\gamma)^{\lfloor S/2 \rfloor}$. Therefore, with probability at least $1 - |\mathcal{N}|(\delta/\gamma)^{\lfloor S/2 \rfloor}$, $\mathbf{m}_1 = \mathbf{0}$ and (27) becomes

$$\frac{\mu(\mathbf{n})}{\tilde{\mu}(\mathbf{n})} = \exp(i\theta_2 - i\theta_1)\frac{\mu^{(2)}(\mathbf{n}+\mathbf{m}_2)f(\mathbf{n}+\mathbf{m}_2)}{\mu^{(2)}(\mathbf{n})f(\mathbf{n})}.$$

Moreover, if $\mu^{(2)}f$ satisfies the non-degeneracy condition, then $\mathbf{m}_2 = \mathbf{0}$, $\tilde{f}(\mathbf{n}) = \exp(i\theta_2)f(\mathbf{n})$, $\forall \mathbf{n}$, and $\tilde{\mu}(\mathbf{n}) = \exp(i\theta_1 - i\theta_2)\mu(\mathbf{n})$, if $f(\mathbf{n}) \neq 0$, with probability at least $1 - |\mathcal{N}|(\delta/\gamma)^{\lfloor S/2 \rfloor}$.

In the case of (23)&(26), we have

$$\exp(i\theta_1)\mu(\mathbf{n}+\mathbf{m}_1)\mu^{(2)}(\mathbf{n})f(\mathbf{n}+\mathbf{m}_1) = \exp(i\theta_2)\tilde{\mu}(\mathbf{n})\overline{\mu^{(2)}(\mathbf{m}_2-\mathbf{n})f(\mathbf{m}_2-\mathbf{n})}. \tag{29}$$

The same argument applies and $\mathbf{m}_1 = 0$ with probability at least $1 - |\mathcal{N}|(\delta/\gamma)^{\lfloor S/2 \rfloor}$, and (29) becomes

$$\frac{\mu(\mathbf{n})}{\tilde{\mu}(\mathbf{n})} = \exp(i\theta_2 - i\theta_1)\frac{\overline{\mu^{(2)}(\mathbf{m}_2-\mathbf{n})f(\mathbf{m}_2-\mathbf{n})}}{\mu^{(2)}(\mathbf{n})f(\mathbf{n})},$$

which violates the non-degeneracy condition. In other words, (23)&(26) holds with probability at most $|\mathcal{N}|(\delta/\gamma)^{\lfloor S/2 \rfloor}$.

Similar conclusions follow in the case of (24)&(25) and (24)&(26). □

Appendix C. Proof of Lemma 1

Proof. Since the operator $\mathcal{T}$ enforces the measured Fourier intensities Y

$$\begin{aligned} r(f_{k+1}, \mu_{k+1}) &= \| \, |\Phi\Lambda_{k+1} f_{k+1}| - Y \, \| \\ &\leq \|\Phi\Lambda_{k+1} f_{k+1} - \mathcal{T}\Phi\Lambda_k f_{k+1}\| = \|\Lambda_{k+1} f_{k+1} - \Phi^{-1}\mathcal{T}\Phi\Lambda_k f_{k+1}\| \end{aligned}$$

by the unitarity of the Fourier transform. By splitting the summation and using the definition (8), the rightmost term becomes

$$\left(\sum_{f_{k+1}(\mathbf{n})\neq 0} |f_{k+1}|^2(\mathbf{n}) \Big| \mu_{k+1}(\mathbf{n}) - \mu'_k(\mathbf{n}) \Big|^2 + \sum_{f_{k+1}(\mathbf{n})=0} \Big| \Phi^{-1}\mathcal{T}\Phi\Lambda_k f_{k+1}(\mathbf{n}) \Big|^2 \right)^{1/2} . \tag{30}$$

Now since $\mu_{k+1}(\mathbf{n}) = \mathcal{Q}_{\mathrm{m}}\mu'_k(\mathbf{n})$ is a pixel-wise projection of $\mu'_k(\mathbf{n})$, $|\mu_{k+1}(\mathbf{n}) - \mu'_k(\mathbf{n})| \leq |\mu_k(\mathbf{n}) - \mu'_k(\mathbf{n})|$ and hence (30) is less than or equal to

$$\begin{aligned} &\leq \left(\sum_{f_{k+1}(\mathbf{n})\neq 0} |f_{k+1}|^2(\mathbf{n}) \Big| \mu_k(\mathbf{n}) - \mu'_k(\mathbf{n}) \Big|^2 + \sum_{f_{k+1}(\mathbf{n})=0} \Big| \Phi^{-1}\mathcal{T}\Phi\Lambda_k f_{k+1}(\mathbf{n}) \Big|^2 \right)^{1/2} \\ &= \|\Lambda_k f_{k+1} - \Phi^{-1}\mathcal{T}\Phi\Lambda_k f_{k+1}\| = \|\Phi\Lambda_k f_{k+1} - \mathcal{T}\Phi\Lambda_k f_{k+1}\| \\ &= \| \, |\Phi\Lambda_k f_{k+1}| - Y \, \| = r(f_{k+1}, \mu_k) \end{aligned}$$

which is the desired result. □

References

[1] H. H. Bauschke, P. L. Combettes and D. R. Luke, "Phase retrieval, error reduction algorithm, and Fienup variants: a view from convex optimization," J. Opt. Soc. Am. A **19**, 13341-1345 (2002).

[2] H. H. Bauschke, P. L. Combettes, and D. R. Luke, "Finding best approximation pairs relative to two closed convex sets in Hilbert spaces," J. Approx. Th. **127**, 178192 (2004)

[3] M. Dierolf, A. Menzel, P. Thibault, P. Schneider, C. M. Kewish, R. Wepf, O. Bunk, and F. Pfeiffer, " Ptychographic x-ray computed tomography at the nanoscale," Nature **467**, 436-439 (2010).

[4] J. Douglas and H.H. Rachford, "On the numerical solution of heat conduction problems in two and three space variables," *Trans. Am. Math. Soc.***82**, 421-439 (1956).

[5] A. Fannjiang, "Absolute uniqueness of phase retrieval with random illumination," Inverse Problems **28**, 075008(2012).

[6] A. Fannjiang and W. Liao, "Phase retrieval with random phase illumination," J. Opt. Soc. A, **29**, 1847-1859(2012).

[7] A. Fannjiang and W. Liao, "Phase retrieval with roughly known mask," arXiv:1212.3858.

[8] J. R. Fienup, "Phase retrieval algorithms: a comparison," Appl. Opt. **21**, 2758-2769 (1982).

[9] J.R. Fienup, "Reconstruction of a complex-valued object from the modulus of its Fourier transform using a support constraint," *J. Opt. Soc. Am. A* **4**, 118 -123 (1987).

[10] J.R. Fienup and C.C. Wackerman, "Phase-retrieval stagnation problems and solutions," *J. Opt. Soc. Am. A* **3** 1897-1907 (1986).

[11] R. W. Gerchberg and W. O. Saxton, "A practical algorithm for the determination of the phase from image and diffraction plane pictures," Optik **35**, 237-246, 1972.

[12] M. Hayes, "The reconstruction of a multidimensional sequence from the phase or magnitude of its Fourier transform," IEEE Trans. Acoust. Speech Sign. Proc. **30** 140- 154 (1982).

[13] M.H. Hayes and J.H. McClellan. "Reducible Polynomials in More Than One Variable." Proc. IEEE **70**(2):197 198, (1982).

[14] P.-L. Lions and B. Mercier,"Splitting algorithms for the sum of two nonlinear operators," SIAM J. Num. Anal. **16**, 964-979 (1979).

[15] A. M. Maiden, M. J. Humphry, F. Zhang and J. M. Rodenburg, "Superresolution imaging via ptychography," J. Opt. Soc. Am. A **28**, 604-612 (2011).
[16] A.M. Maiden, G.R. Morrison, B. Kaulich, A. Gianoncelli & J.M. Rodenburg, "Soft X-ray spectromicroscopy using ptychography with randomly phased illumination," *Nat. Commun.* **4**, 1669 (2013).
[17] J. Miao, P. Charalambous, J. Kirz and D. Sayre, "Extending the methodology of X-ray crystallography to allow imaging of micrometre-sized non-crystalline specimens," Nature **400**, 342–344 (1999).
[18] J. Miao, J. Kirz and D. Sayre, "The oversampling phasing method," Acta Cryst. D **56**, 1312–1315 (2000).
[19] J. Miao, D. Sayre and H.N. Chapman, "Phase retrieval from the magnitude of the Fourier transforms of nonperiodic objects," *J. Opt. Soc. Am. A* **15** 1662-1669 (1998).
[20] K.A. Nugent, A.G. Peele, H.N. Chapman, & A.P. Mancuso, "Unique Phase Recovery for Nonperiodic Objects," *Phys. Rev. Lett.* **91**, 203902 (2003).
[21] K. A. Nugent, A. G. Peele, H. M. Quiney and H. N. Chapman, "Diffraction with wavefront curvature: a path to unique phase recovery," *Acta Crystallogr. Sect. A* **61**, 373-381 (2005).
[22] P. Thibault, M. Dierolf, A. Menzel, O. Bunk, C. David, F. Pfeiffer, "High-resolution scanning X-ray diffraction microscopy", Science **321**, 379-382 (2008).
[23] P. Thibault, M. Dierolf, O. Bunk, A. Menzel, F. Pfeiffer, "Probe retrieval in ptychographic coherent diffractive imaging," Ultramicroscopy **109**, 338343 (2009)
[24] G. J. Williams, H. M. Quiney, B. B. Dhal, C. Q. Tran, K. A. Nugent, A. G. Peele, D. Paterson, and M. D. de Jonge, "Fresnel coherent diffractive imaging", *Phys. Rev. Lett.* **97**, 025506(2006).
[25] F. Zhang and J. M. Rodenburg, "Phase retrieval based on wave-front relay and modulation," *Phys. Rev. B* **82**, 121104(R) (2010).

Department of Mathematics, University of California, Davis, CA 95616